Structure and Electronic Transitions of $C7H_4O_2^+$ and $C_7H_5O_2^+$ Ions; Neon Matrix and Theoretical Studies

Journal:	*The Journal of Physical Chemistry*
Manuscript ID	jp-2016-10687s.R1
Manuscript Type:	Article
Date Submitted by the Author:	30-Nov-2016
Complete List of Authors:	Fulara, Jan; Polish Academy of Sciences, Institute of Physics Erattupuzha, Sonia; University of Basel, Chemistry Garkusha, Iryna; University of Basel, Chemistry Maier, John; University of Basel, Department of Chemistry

Structure and Electronic Transitions of $C_7H_4O_2^+$ and $C_7H_5O_2^+$ Ions; Neon Matrix and Theoretical Studies

Jan Fulara*[,†,‡] Sonia Erattupuzha[†,§] , Iryna Garkusha[†] and John P. Maier[†]

[†]Department of Chemistry, University of Basel, Klingelbergstrasse 80, CH-4056, Basel, Switzerland

[‡]Institute of Physics, Polish Academy of Sciences, Al. Lotników, 32/46, PL-02-668 Warsaw, Poland

Abstract

$C_7H_4O_2^+$ and $C_7H_5O_2^+$ ions and the respective neutrals have been investigated by absorption spectroscopy in neon matrices following mass-selection of ions produced from salicylic acid. Three electronic transitions starting at 649.6, 431.0 and 372.0 nm are detected for $C_7H_4O_2^+$ and assigned on the basis of CASPT2 energies and Franck-Condon simulations as the excitations from the $X\,^2A''$ to the $1\,^2A''$, $2\,^2A''$ and $3\,^2A''$ electronic states of 6-(oxomethylene)-2,4-cyclohexadien-1-one ion ($\mathbf{A}^+$). Absorptions commencing at 366.4 nm are observed for $C_7H_5O_2^+$ and assigned to the $1\,^2A' \leftarrow X\,^2A'$ electronic transition of (2-hydroxyphenyl)methanone ion ($\mathbf{J}^+$). Neutralization of $\mathbf{J}^+$ leads to the appearance of four absorption systems attributed to the $4\,^2A''$, $3\,^2A''$, $2\,^2A''$, $1\,^2A'' \leftarrow X\,^2A''$ transitions of **J** with origin bands 291.3, 361.2, 393.8, and 461.2 nm.

Introduction

Partially oxygenated hydrocarbons are pollutants of Earth's atmosphere, emitted for example by traffic and biomass burning. Another source of these species are volatile hydrocarbons of biogenic and anthropogenic origin, which are oxidized or photo-oxidized by NO_x, O_3 and OH in the atmosphere.[1-3] The oxygenation products, being less volatile than the hydrocarbon precursors, contribute to the formation of secondary organic aerosols (SOA).[4-7] SOA may affect human health and the climate. As was demonstrated for several hydrocarbons[8-11] (toluene, xylenes, ethyl-benzenes constituting a major fraction of hydrocarbons emitted in urban air) and natural terpenes[12] a complex chemistry takes place during formation of SOA leading to cyclic and open chain ketones, aldehydes, alcohols and carboxylic acids.

To model oxidation of hydrocarbons in the atmosphere or combustion a knowledge of the structure and energetics of the intermediates is needed. The phenoxy and benzoyl radicals are just two model compounds, which have been the topic of studies in the past decades. Photolysis of phenol or anisole is a popular way for production of $C_6H_5O^{\bullet}$. The mechanism of photo-dissociation of phenol has been studied theoretically[13] and by photo-fragment translational spectroscopy.[14-15] $C_6H_5O^{\bullet}$ has been characterized by electron spin resonance, infrared, resonance-enhanced Raman and UV/Vis spectroscopies, which have been reviewed.[16, 17]

Benzoyl radical ($C_6H_5CO^{\bullet}$) is an important intermediate in combustion and atmosphere. Burning of light aromatic hydrocarbons under oxygen deficient conditions leads to formation of the phenyl radical and CO, the association of which produces $C_6H_5CO^{\bullet}$. Kinetics of this reaction were studied[18] and of the reverse process thirty years earlier.[19] Benzaldehyde is the source of $C_6H_5CO^{\bullet}$ in the atmosphere; it readily loses a hydrogen atom in the reaction with OH or NO_x.[20] Benzoyl radical once formed reacts fast with molecular

oxygen.[21,22] In the laboratory, benzoyl is most frequently produced by the UV induced α–cleavage of aromatic carbonyls and can be tracked by the strongest IR band at ~1840 cm^{-1},[23-25] as the UV transition around 310 nm is weak.[26]

Phenoxy and benzoyl ions, closed – shell electronic systems, have been less explored than the respective neutrals. $C_6H_5O^+$ was generated in non-aqueous solutions by multiphoton ionization of phenol and transient absorptions in the UV were measured.[27] Phenoxide anion was studied by photodetachment spectroscopy.[16] Infrared[28] and electronic spectra of benzoyl cation produced in a superacidic environment[29,30] and gas-phase[30] have been reported. $C_6H_5CO^+$ was also detected in the infrared following the associative recombination of phenyl cation with CO in an argon matrix.[31] The benzoyl cation,[32] and its weakly – bound clusters with argon and H_2O,[33] have been investigated in the gas phase *via* infrared spectroscopy.

In this contribution the electronic absorption spectra of $C_7H_4O_2^+$, $C_7H_5O_2^+$, and their neutrals measured in 6 K neon matrices following mass – selective deposition are reported. The ions possess two functional groups: oxo-, characteristic for the phenoxy cation, and =CO, occurring in the benzoyl cation linking these two intermediates. The here presented results provide a good starting point for gas phase investigations of such species, which are likely important intermediates produced in ionizing fragmentation of hydroxycarboxylic acids; the components of SOA.

Methods

Experimental

A mixture of $C_7H_4O_2^+$, $C_7H_5O_2^+$ and other ions was produced from the vapor of salicylic acid premixed with helium in a hot - cathode ion source. Ions were extracted and guided through an electrostatic bender, to rid of neutrals, into a quadrupole mass filter (QMF). After passing the QMF the ion beam 17 nA of $C_7H_4O_2^+$, or 13 nA of $C_7H_5O_2^+$ was co-

deposited with neon contaminated with CH_3Cl in the ratio 20000:1 onto a sapphire substrate coated with rhodium held at 6 K. CH_3Cl acts as an electron scavenger which improves the collection efficiency of ions. A 150 μm thick matrix was grown during 4 hours for $C_7H_4O_2^+$ and 3.5 hours in the case of $C_7H_5O_2^+$ resulting in accumulation of 220 and 170 μC of ions, respectively. After the matrix growth is completed, absorption spectra of trapped species are measured using a halogen or xenon lamp, a 0.3 m spectrometer and a CCD camera. Broad-band light passed through the thin side of solid neon parallel to the substrate, was collected and guided *via* a bundle of quartz fibers to the spectrograph. The spectra were collected in several overlapping sections of ~70 nm. To distinguish absorptions of ions from those of neutrals the matrix was exposed for 30 min to $\lambda > 260$ nm photons. The photons liberate electrons from Cl^-, themselves formed from CH_3Cl and recombine with cations forming the neutrals. In the spectrum measured under such conditions the bands originating from cations diminish and the ones which grow in intensity belong to neutrals.

Computational

Several isomers of $C_7H_4O_2^+$ (Chart 1) and $C_7H_5O_2^+$ (Chart 2) were chosen for computational studies according to their stability. Calculations have been carried out with the density functional method (DFT) using the M06-2X functional[34] and cc-pVTZ basis set[35] supplemented in the Gaussian 09 software.[36] Harmonic vibrational frequencies have been computed to test whether the obtained structures possess real minima. Vertical excitation energies and oscillator strengths for ions and respective neutrals have been computed using the time dependent (TD) DFT and multistate, multi-configurational second order perturbation (MS-CASPT2)[37] methods at the coordinates obtained from M06-2X/cc-pVTZ. For the latter the Molcas 8 program package[38] was exploited. An active space in the CASPT2 calculation was built of eleven electrons distributed on twelve orbitals for $C_7H_4O_2^+$ and 12/12 for $C_7H_5O_2^+$. Vibrational frequencies, needed for Franck-Condon simulations of the electronic

spectra, have been computed at a smaller active space (seven electrons on 8 orbitals for $C_7H_4O_2^+$) or at lower level of theory: multiconfigurational complete active space (CAS) for $C_7H_5O_2^+$ or TD DFT for its neutral. This was dictated by difficulties in geometry optimization in the excited electronic state of the ion, or much larger computational costs for a given species at lower symmetry.

Results and discussion

$C_7H_4O_2^+$

$C_7H_4O_2^+$ is the dominant ion in the mass spectrum of salicylic acid (Figure 1SI). Deposition of *m/z* 120 ions into neon results in strong absorptions in the visible and UV (blue trace Figure 1). Three electronic systems starting around 650, 431 and 372 nm diminished with UV ($\lambda > 260$ nm) irradiation of the matrix (red trace) pointing to cationic origin of these absorptions; namely $C_7H_4O_2^+$. Only one moderately intense band at 453 nm gained intensity and therefore corresponds to neutral $C_7H_4O_2$.

To infer the structure of the $C_7H_4O_2^+$ ion, the carrier of the three absorption systems, calculations of the ground state energies of several isomers were carried out at the M06-2X/cc-pVTZ level and the results are given in Chart 1. The most stable is 6-(oxomethylene)-2,4-cyclohexadien-1-one ion (structure $\mathbf{A}^+$). Isomer $\mathbf{C}^+$ with the oxomethylene group in the para position is ~33 kJ/mol less stable. Three isomers of $C_7H_4O_2^+$: $\mathbf{F}^+$, $\mathbf{G}^+$ and $\mathbf{H}^+$ contain a pyrane or furan ring and thus differ significantly from the structure of the precursor used. $\mathbf{G}^+$ and $\mathbf{H}^+$ are the parent ions of stable molecules. $\mathbf{D}^+$ and $\mathbf{E}^+$ can be formed in the ion source by a ring opening of the precursor.

All isomers (Chart 1) except the two highest – energy ones with a furanyl group: $\mathbf{G}^+$ and $\mathbf{H}^+$, were chosen for excitation energies calculations. These were carried out with MS(6)-CASPT2 (11,12) using coordinates from M06-2X/cc-pVTZ computations and

cc-pVTZ basis set for all atoms. The results are given in Table 1SI. Two ions $\mathbf{A}^+$ and $\mathbf{F}^+$ possess electronic transitions with energies close to the absorption systems at 650 (1.91 eV) , 431 (2.88 eV) and 372 (3.33 eV) nm. The f value of the second transition of $\mathbf{F}^+$ is however smaller than the first one, in contrast to the observation. In the case of $\mathbf{A}^+$, not only the energies, but also the oscillator strength (f) of the first three electronic transitions match well the spectrum of $C_7H_4O_2^+$.

$C_7H_4O_2^+$ is produced in the ion source by elimination of water from *o*-hydroxybenzoic acid ion (Figure 1SI). $\mathbf{A}^+$ and $\mathbf{B}^+$ have a similar arrangement of atoms to salicylic acid. $\mathbf{A}^+$ is formed by recombination of OH from a carboxylic group with hydrogen atom adjacent to it, whereas in case of $\mathbf{B}^+$ hydrogen comes from the benzene ring. $\mathbf{B}^+$ can be excluded as the carrier of new cationic absorptions shown in the blue trace of Figure 1, because the calculated excitation energies (Table 1SI) do not match. Taking into account the similarity of structure $\mathbf{A}^+$ and salicylic acid, the fact that $\mathbf{A}^+$ is the lowest energy isomer of $C_7H_4O_2^+$, and the energy and intensity agreement of the computed (Table 1SI) with the experimental spectrum, the absorptions starting at 650, 431 and 372 nm are assigned to the $1\,^2A'' \leftarrow X\,^2A''$, $2\,^2A'' \leftarrow X\,^2A''$ and $3\,^2A'' \leftarrow X\,^2A''$ transitions of this $C_7H_4O_2^+$ isomer.

The observed electronic transitions of A^+ result from the excitations of electrons residing on π orbitals of a'' symmetry (Figure 3SI). The main electronic configuration of the ground state, with the reference weight (r.w.) 0.82, is: …$1a''^2 2a''^2 3a''^2 26a'^2 4a''^2 5a''^1$. Promotion of an electron from the 4a'' to 5a'' orbital is responsible for the absorptions starting at 650 nm. The next electronic transition to the $2\,^2A''$ is due to the 3a'' to 5a'' excitation. The $3\,^2A''$ electronic state has the main $1a''^2 2a''^2 3a''^2 4a''^2 5a''^0 6a''^1$ configuration with r.w. 0.56 (see comments to Fig. 3SI).

The calculated excitation energies of $\mathbf{A}^+$ are compared in Table 1 with the experimental data. These overestimate the energies by ~ 0.3 eV. The adiabatic energies should match the observations better. To test this MS(4)-CASPT2 calculations of vertical excitation energies at a smaller active space (seven electrons distributed on eight orbitals) and a smaller basis set (cc-pVDZ) were carried out using the coordinates from the M06-2X/cc-pVTZ computations. The three lowest energy transitions are predicted at 2.33, 3.25 and 3.70 eV with f values 0.023, 0.1 and 0.15. The computed electronic spectrum does not differ much from that obtained with the higher level calculations (Table 1SI). The coordinates of $C_7H_4O_2^+$ in the ground and 1 ^{2}A", 2 ^{2}A" and 3 ^{2}A" electronic states have been optimized at the MS(4)-CASPT2(7/8)/cc-pVDZ level and the resulting adiabatic energies are 2.02, 2.91 and 3.44 eV. These are lower by ~ 0.3 eV from the vertical ones and close to the observations (Table 1).

The frequencies of 23 totally symmetric vibrations have been computed with MS(4)-CASPT2(7/8)/cc-pVDZ using the equilibrium coordinates of $\mathbf{A}^+$ in the X ^{2}A", 1 ^{2}A", 2 ^{2}A" and 3 ^{2}A" states and are given in Table 2SI. These are compared there with the M06-2X/cc-pVTZ computations and are close to each other. The CASPT2 frequencies, the equilibrium coordinates and L-matrices in the ground and three excited electronic states of $\mathbf{A}^+$ were used for the Franck-Condon (F-C) simulation of the matrix spectrum of $C_7H_4O_2^+$ with the Pgopher program.[39] The stick and the broader (200 cm^{-1}) Gaussian profiles spectra of $\mathbf{A}^+$ are compared in Figure 2 with the experiment. The theoretical spectra of $\mathbf{A}^+$ mimic to some extent the experiment and strengthen the assignment. The wavelengths of the absorption bands of 6-(oxomethylene)-2,4-cyclohexadien-1-one ion ($\mathbf{A}^+$) with the assignment based on the calculated electronic excitation energies, CASPT2 vibrational frequencies and F-C simulations are given in Table 2.

A broad absorption at 453 nm (2.74 eV) seen in Figure 1, which grows after irradiation of the matrix with UV photons (λ > 260 nm), belongs to neutral **A**. Calculations at the MS(5)-CASPT2(12/12)/cc-pVTZ level predict a strong $1\ ^1A' \leftarrow X\ ^1A'$ electronic transition at 3.55 eV. Next transition lies at 5.0 eV. Though the calculated vertical excitation energy overestimates the observation by ~0.8 eV, the 453 nm band is assigned to the $1\ ^1A' \leftarrow X\ ^1A'$ electronic transition of **A**, because $\mathbf{A}^+$ is present in the matrix and **A** is the neutralization product.

$C_7H_5O_2^+$ and $C_7H_5O_2$

A weak peak of *m/z* 121 is apparent in the mass spectrum of *o*-hydroxybenzoic acid (Figure 1SI). $C_7H_5O_2^+$ is produced in the ion source by elimination of OH from the parent ion. On the other hand the *m/z* 121 ion dominates mass spectra of *meta*- and *para*-hydroxybenzoic acids,[40] whereas *m/z* 120 is absent (Figure 1SI). The $[M - OH]^+$ ions are prevalent in mass-spectra of benzoic (Figure 1SI) and other carboxylic acids.

Though the intensity of the *m/z* 121 ion in the mass spectrum of *o*-hydroxybenzoic acid is about eight times lower than the '120' ion nevertheless this precursor was used for generation of the '121' ions. After optimization of the production conditions it was possible to attain an average current of 13 nA for *m/z* 121, and 17 nA for *m/z* 120.

The spectrum measured after accumulation ~170 μC of the '121' ions in neon is shown as the blue trace in Figure 3 and the one recorded after 30 min irradiation of the matrix with λ > 260 nm photons in the red trace. The absorptions commencing at 366 nm, which vanish after the UV irradiation are cationic in nature and correspond to $C_7H_5O_2^+$, whereas the new ones which appeared belong to the neutral counterpart.

To deduce the arrangement of the atoms in this $C_7H_5O_2^+$ isomer responsible for the 366 nm electronic system, five plausible structures ($\mathbf{J}^+$ - $\mathbf{N}^+$) were chosen for quantum

calculations (Chart 2). All considered ions, except $\mathbf{M}^+$, possess the same skeleton as **A**, and differ in the protonation site. Calculations with M06-2X/cc-pVTZ reveal that $\mathbf{J}^+$ with hydrogen attached to the oxygen atom is the global minimum and the next in energy ion, $\mathbf{K}^+$, protonated at the benzene ring in the position adjacent to carbonyl group, lies ~84 kJ/mol above it.

$C_7H_5O_2^+$ ions are closed shell species with a singlet ground state and therefore the time dependent (TD) DFT method could be used for computation of the vertical excitation energies, Table 3SI. According to the DFT calculations only $\mathbf{J}^+$ and $\mathbf{K}^+$ possess a strong electronic transition at 4.0 or 3.9 eV, close to the origin of the 366 nm (3.38 eV) system. To confirm this, calculations with MS(4)-CASPT2(12/12)/cc-pVTZ were carried out for $\mathbf{J}^+$ and $\mathbf{K}^+$ and the results are compared with the DFT ones in Table 3SI. The CASPT2 excitation energy to the first excited ^{1}A' electronic state is 3.87 and 3.69 eV for $\mathbf{J}^+$ and $\mathbf{K}^+$, respectively, close to the DFT prediction. According to the calculations, a stronger transition is expected to the second ^{1}A' electronic state for both ions, which lies 5 eV above the X state and out of the range of the detection system.

To determine which ion is the carrier of the absorptions commencing at 366 nm, F-C simulations of the vibrational pattern in the $1\ ^1A' \leftarrow X\ ^1A'$ transition of both ions were carried out. For this purpose vibrational frequencies of 25 totally symmetric normal modes were computed at the MS(4)-CAS(8/8)/cc-pVDZ level using the equilibrium coordinates calculated at the same level. The ground state frequencies of $\mathbf{J}^+$ obtained are compared with the M06-2X/cc-pVTZ and MS(4)-CASPT2(8/8)/cc-pVDZ ones in Table 4SI. The DFT and CASPT2 frequencies agree well, but those obtained with the CAS method are systematically higher for all vibrational modes. A linear dependence of the CAS versus CASPT2 frequencies is observed with the slope 1.05. Vibrational frequencies in the $1\ ^1A'$ electronic state of $\mathbf{J}^+$

from the CASPT2 method could not be obtained due to convergence problems during geometry optimization.

The CAS frequencies scaled by 0.95 (1/1.05) result in a better agreement with the values obtained from the two other methods (Table 4SI). These frequencies in the X ^{1}A' and 1 ^{1}A' electronic states were then used for the simulation of the electronic spectra of $\mathbf{J}^+$ and $\mathbf{K}^+$. The stick and Gaussian (200 cm^{-1}) profile spectra are compared in Figure 4 with the matrix spectrum of $C_7H_5O_2^+$. The theoretical spectrum of $\mathbf{J}^+$ resembles the 366 nm electronic system, whereas that one of $\mathbf{K}^+$ differs. Therefore the new absorptions with the origin at 366 nm are assigned to the 1 ^{1}A' ← X ^{1}A' electronic transition of $\mathbf{J}^+$. Scaling of the CAS frequencies has no effect on the appearance of the theoretical spectrum of $\mathbf{J}^+$ as one can see in Figure 2SI. In the ground ^{1}A' state all (1-26) a' orbitals and all π orbitals (1-5) of a" symmetry are doubly occupied (Fig. 4SI). The 1 ^{1}A' state results from the two major electronic configurations: …(3a")^2(4a")^2(5a")^1(6a")^1 and …(3a")^2(4a")^1(5a")^2(6a")^1 with the reference weight 0.36 and 0.33, respectively (Fig. 4SI).

The F-C simulation guided the assignment of the bands in the electronic spectrum of $\mathbf{J}^+$. The frequencies derived and listed in Table 2 do not correspond to an individual vibration but are the average of several due to broadening and congestion (Figure 4). The F-C simulations suggest which vibrational modes are the main contributors to a given absorption band.

Two weak absorptions (blue trace in Figure 3) starting at ~ 435 nm (2.85eV) and 320 nm (3.87 eV) belong likely to a minor isomer of $C_7H_5O_2^+$. The best candidate for the carrier of these bands is isomer $\mathbf{N}^+$ possessing two relatively strong 1 ^{3}A' ← X ^{3}A' and 1 ^{3}A' ← X ^{3}A' electronic transitions close to these energies (3,17 and 4.22 eV, Table 3SI).

Four band systems appeared after neutralization of $\mathbf{J}^+$ with $\lambda > 260$ nm photons (red trace in Figure 3). These are: weak absorptions starting at 461 nm, two moderately intense

ones with onsets at 394 and 361 nm and the strong system with origin at 291 nm. The structureless short-wavelength tail below 250 nm is likely artificial and may result from the enhanced light scattering in this region and lack of background correction. The four absorption systems belong to **J** because they appeared after neutralization of $\mathbf{J}^+$.

To confirm this interpretation vertical excitation energies and oscillator strengths of **J** have been calculated at the MS(8)-CASPT2(9/9)/cc-pVDZ level, Table 5SI. The calculations predict three moderately intense transitions at 2.48, 3.38 and 3.83 eV and a strong one at 4.99 eV. The results are compared with the observations in Table 1. The energy of the 461 nm (2.69 eV) system is underestimated by ~ 0.2 eV, whereas the three other at 394 nm (3.15 eV), 361 nm (3.43 eV) and 291 nm (4.26 eV) are overestimated by 0.2 - 0.7 eV. Computation of the adiabatic energies of **J** was not successful due to problems with geometry optimization at the CASPT2 level. The OH group of molecule tends to move out of plane and calculations at the C_1 symmetry are time consuming.

Instead of CASPT2, TD DFT calculations were carried out. Vertical excitation energies and the f values obtained are compared with the CASPT2 ones in Table 5SI. The TD DFT energies are ~ 0.2 eV larger. Both methods predict similar oscillator strengths. The adiabatic energies of **J** at the M06-2X/TDDFT/cc-pVTZ level are given in Table 5SI. These are lower by 0.3-0.6 eV than the vertical ones. The adiabatic energy of the $4\,^2A''$ state could not be computed due to convergence problems. Besides the adiabatic energies the calculations provide frequencies of normal modes in the ground and excited electronic states of J, Table 6SI.

Based on the theoretical calculations the four electronic systems of **J** at: 461, 394, 361 and 291 nm are assigned to the $1\,^2A'' \leftarrow X\,^2A''$, $2\,^2A'' \leftarrow X\,^2A''$, $3\,^2A'' \leftarrow X\,^2A''$, $4\,^2A'' \leftarrow X\,^2A''$ electronic transitions. In the CASPT2 calculations the active space was built only of π orbitals, and these are shown in Figure 6SI. The main electronic configurations of

the ground and the 1-4 ^{2}A″ excited electronic states are also discussed in the SI. The assignment of the vibrational bands in the spectrum of **J** (Table 2) is assisted with frequencies computed with the TD DFT method (Table 6SI) except the $4\,^2A'' \leftarrow X\,^2A''$ electronic transition for which F-C simulations have been carried out (Figure 6SI) using the CASSCF equilibrium gemoetries, L-matrices and frequencies.

Conclusions

The structure, symmetry and energetics of the ground and excited electronic states of the $C_7H_4O_2^+$ and $C_7H_5O_2^+$ fragment ions produced from salicylic acid have been studied by electronic spectroscopy of mass selected ions trapped in solid neon and by theoretical methods. Three electronic absorption systems are observed for $C_7H_4O_2^+$. These are identified on the basis of CASPT2 energies and the F-C vibrational profiles as the electronic excitations from the $X\,^2A''$ state to the $1\,^2A''$, $2\,^2A''$, $3\,^2A''$ electronic states of the 6-(oxomethylene)-2,4-cyclohexadien-1-one ion ($\mathbf{A}^+$).

Deposition into neon of *o*-hydroxy-benzoic acid *m/z* 121 ion resulted in strong absorptions of $C_7H_5O_2^+$ in the UV region. On the basis of calculated excitation energies and F-C simulations, it is shown that the new absorption system originates from the $1\,^1A' \leftarrow X\,^1A'$ electronic transition of (2-hydroxyphenyl)methanone ion ($\mathbf{J}^+$). Four electronic transitions have been observed in a neon matrix for $\mathbf{J}^\bullet$ following neutralization of $C_7H_5O_2^+$ and identified as the excitations from the $X\,^2A''$ state to the $1\,^2A''$, $2\,^2A''$, $3\,^2A''$, $4\,^2A''$ electronic states.

The arrangement of atoms in $\mathbf{A}^+$ and $\mathbf{J}^+$ explains the different fragmentation of *o*-hydroxybenzoic acid ion in comparison to the *meta*- and *para*- isomers. In the former two fragmentation channels are open: elimination of OH or H_2O where the second one prevails, whereas for the *meta*- and *para*- only the first pathway is accessible.

The reported spectroscopic data on $C_7H_4O_2^+$, $C_7H_5O_2^+$, $C_7H_4O_2$ and $C_7H_5O_2$ can be used as a starting point for gas-phase studies of these species, ionic fragments of aromatic hydroxycarboxylic acids which are important constituents of secondary organic aerosols.

Associated content

Supporting Information

The Supporting Information is available free of charge on the ASC Publications website at DOI:

Mass spectra of benzoic and *o*-, *m*- and *p*-hydroxybenzoic acids, Franck-Condon simulations of the electronic transitions for isomers $\mathbf{J}^+$ and $\mathbf{K}^+$ using unscaled CAS frequencies, F-C simulation of the $4\,^2A'' \leftarrow X\,^2A''$ electronic transition of $\mathbf{J}^\bullet$, the HOMO-LUMO orbitals of $\mathbf{A}^+$, $\mathbf{J}^+$ and $\mathbf{J}^\bullet$, vertical excitation energies and oscillator strengths of $C_7H_4O_2^+$ and $C_7H_5O_2^+$ ions and $C_7H_5O_2$ ($\mathbf{J}^\bullet$), totally symmetric vibrational frequencies of $\mathbf{A}^+$, $\mathbf{J}^+$ and $\mathbf{J}^\bullet$ and full reference 36.

Author Information

Corresponding Author

*J. Fulara. E-mail: fulara@ifpan.edu.pl

Present Address

[§]S. Erattupuzha. Photonics Institute, TU Wien, A-1040 Vienna, Austria.

Notes

The authors declare no competing financial interest.

Acknowledgement

This work was supported by the Swiss National Science Foundation (project no. 200020-124349/1). Calculations were performed at sciCORE (http://scicore.unibas.ch/) scientific computing core facility at University of Basel.

References

(1) Kavouras, I. G.; Mihalopoulos, N.; Stephanou, E. G. Formation of Atmospheric Particles from Organic Acids Produced by Forests. *Nature* **1998**, *395*, 683-686.

(2) Odum, J. R.; Jungkamp, T. P. W.; Griffin, R. J.; Flagan, R. C.; Seinfeld, J. H. The Atmospheric Aerosol-Forming Potential of Whole Gasoline Vapor. *Science* **1997***, 276*, 96-99.

(3) O'Dowd, C. D.; Aalto, P.; Hämeri, K.; Kulmala, M.; Hoffmann, T. Atmospheric Particles from Organic Vapours. *Nature* **2002**, *416*, 497-498.

(4) Zhang, R.; Suh, I.; Zhao, J.; Zhang, D.; Fortner, E. C.; Tie, X.; Molina, L. T.; Molina, M. J. Atmospheric New Particle Formation Enhanced by Organic Acids. *Science* **2004**, *304*, 1487-1490.

(5) Tu, P.; Hall, W. A.; Johnston, M. V. Characterization of Highly Oxidized Molecules in Fresh and Aged Biogenic Secondary Organic Aerosol. *Anal. Chem.* **2016**, *88*, 4495−4501.

(6) Lopez-Hilfiker, F. D.; Mohr, C.; D'Ambro, E. L.; Lutz, A.; Riedel, T. P.; Gaston, C. J.; Iyer, S.; Zhang, Z.; Gold, A.; Surratt, J. D.; Lee, B. H.; Kurten, T.; Hu, W.W.; Jimenez, J.; Hallquist, M.; Thornton, J. A. Molecular Composition and Volatility of Organic Aerosol in the Southeastern U.S.: Implications for IEPOX Derived SOA. *Environ. Sci. Technol*. **2016**, *50*, 2200−2209.

(7) Forstner, H. J. L.; Flagan, R. C.; Seinfeld, J. H. Secondary Organic Aerosol from the Photooxidation of Aromatic Hydrocarbons: Molecular Composition. *Environ. Sci. Technol.* **1997**, *31*, 1345-1358.

(8) Jang, M.; Kamens, R. M. Characterization of Secondary Aerosol from the Photooxidation of Toluene in the Presence of NO_x and 1-Propene. *Environ. Sci. Technol*. **2001**, *35*, 3626-3639.

(9) Sato, K.; Hatakeyama, S.; Imamura, T.; Secondary Organic Aerosol Formation during the Photooxidation of Toluene: NO_x Dependence of Chemical Composition. *J. Phys. Chem. A* **2007**, *111,* 9796-9808.

(10) Suh, I.; Zhang, R.; Molina, L. T.; Molina, M. J.; Oxidation Mechanism of Aromatic Peroxy and Bicyclic Radicals from OH-Toluene Reactions. *J. Am. Chem. Soc.* **2003**, *125*, 12655-12665.

(11) Sato, K.; Takami, A.; Kato, Y.; Seta, T.; Fujitani, Y.; Hikida, T.; Shimono, A.; Imamura, T. AMS and LC/MS Analyses of SOA from the Photooxidation of Benzene and 1,3,5-trimethylbenzene in the Presence of NO_x: Effects of Chemical Structure on SOA Aging. *Atmos. Chem. Phys*. **2012**, *12*, 4667–4682.

(12) Kameel, F. R.; Hoffmann, M. R.; Colussi, A. J. OH Radical-Initiated Chemistry of Isoprene in Aqueous Media. Atmospheric Implications. *J. Phys. Chem. A* **2013**, *117*, 5117−5123.

(13) Sobolewski, A. L.; Domcke, W. Photoinduced Electron and Proton Transfer in Phenol and Its Clusters with Water and Ammonia. *J. Phys. Chem. A* **2001,** *105,* 9275-9283.

(14) Ashfold, M. N. R.; Cronin, B.; Devine, A. L.; Dixon, R. N.; Nix, M. G. D. The Role of πσ* Excited States in the Photodissociation of Heteroaromatic Molecules. *Science* **2006**, *312***,** 1637-1640.

(15) Nix, M. G. D.; Devine, A. L.; Cronin, B.; Dixon, R. N.; Ashfold ,M. N. R. High Resolution Photofragment Translational Spectroscopy Studies of the Near Ultraviolet Photolysis of Phenol. *J. Chem. Phys.* **2006**, *125*, 133318.

(16) Kim, J. B.; Yacovitch, T. I.; Hock, C. ; Neumark, D. M. Slow Photoelectron Velocity-Map Imaging Spectroscopy of the Phenoxide and Thiophenoxide Anions. *Phys. Chem. Chem. Phys.* **2011**, *13*, 17378–17383.

(17) Cheng, C.- W.; Witek, H.; Lee, Y.- P. Rovibronic Bands of the $\tilde{A}\ ^2B_2 \leftarrow \tilde{X}\ ^2B_1$ Transition of C_6H_5O and C_6D_5O Detected with Cavity Ringdown Absorption near 1.2 μ m. *J. Chem. Phys.* **2008**, *129*, 154307.

(18) Nam, G.- J.; Xia, W.; Park, J.; Lin, M. C. The Reaction of C_6H_5 with CO: Kinetic Measurement and Theoretical Correlation with the Reverse Process. *J. Phys. Chem. A* **2000**, *104,* 1233-1239.

(19) Solly, R. K.; Benson, S. W. Kinetics of the Gas-Phase Unimolecular Decomposition of the Benzoyl Radical. *J. Am. Chem. Soc.* **1971**, *93*, 2127 – 2131.

(20) Atkinson, R. Atmospheric chemistry of VOCs and NO_x. *Atmos. Environ.* **2000**, *34*, 2063-2101.

(21) Sebbar, N.; Bozzelli, J. W.; Bockhorn, H. Thermochemistry and Reaction Paths in the Oxidation Reaction of Benzoyl Radical: $C_6H_5C^{\bullet}(=O)$. *J. Phys. Chem. A* **2011**, *115*, 11897–11914.

(22) Caralp, F.; Foucher, V.; Lesclaux, R.; Wallington, T. J.; Hurley, M. D. Atmospheric Chemistry of Benzaldehyde: UV Absorption Spectrum and Reaction Kinetics and Mechanisms of the $C_6H_5C(O)O_2$ Radical. *Phys. Chem. Chem. Phys.* **1999**, *1*, 3509-3517.

(23) Lin, S.- Y.; Lee, Y.- P. Infrared Absorption of Gaseous Benzoyl Radical C_6H_5CO Recorded with a Step-Scan Fourier-Transform Spectrometer. *J. Phys. Chem. A* **2012**, *116*, 6366−6374.

(24) Neville, A. G.; Brown, C. E.; Rayner, D. M.; Lusztyk, J.; Ingold, K. U. First Direct Detection of Transient Organic Free Radicals in Solution by Time-Resolved Infrared Spectroscopy. Kinetic Studies on Some Acyl Radicals. *J. Am. Chem. Soc.* **1991**, *113*, 1869-1870.

(25) Mardyukov, A.; Sander, W. Matrix Isolation and IR Characterization of the Benzoyl and Benzoylperoxy Radicals. *Eur. J. Org. Chem.* **2010**, 2904–2909.

(26) Huggenberger, C.; Lipscher, J.; Fischer, H. Self-Termination of Benzoyl Radicals to Ground- and Excited-State Benzil. Symmetry Control of a Radical Combination. *J. Phys. Chem.* **1980**, *84*, 3467-3474.

(27) Siuzdak, G.; North, S.; BelBruno, J. J. Multiphoton Ionization of Phenol in Nonaqueous Solutions: Characterization of the Cation and Ion-Molecule Chemistry. *J. Phys. Chem*. **1991**, *95*, 5186-5190.

(28) Olah, G. A.; Kuhn, S. J.; Tolgyesi, W. S.; Baker, E. B. Stable Carbonium Ions. II. Oxocarbonium (Acylium) Tetrafluoroborates, Hexafluorophosphates, Hexafluoro-antimonates and Hexafluoroarsenates. Structure and Chemical Reactivity of Acyl Fluoride : Lewis Acid Fluoride Complexes. *J. Am. Chem. Soc.* **1962**, *84*, 2733-2740.

(29) Olah, G. A.; Pittman, C. U. Jr.; Waack, R.; Doran, M. The Electronic Spectra of Carbonium Ions in Strongly Acidic Solutions. *J. Amer. Chem. Soc.* **1966**, *88*, 1488-1495.

(30) Freiser, B. S.; Beauchamp, J. L. Photochemistry of Organic Ions in the Gas Phase. Comparison of the Gas Phase Photodissociation and Solution Absorption Spectra of Benzoyl Cation, Protonated Benzene, and Protonated Mesitylene. *J. Am. Chem. Soc.***1976**, *98*, 3136-3139.

(31) Winkler, M.; Sander, W. Generation and Reactivity of the Phenyl Cation in Cryogenic Argon Matrices: Monitoring the Reactions with Nitrogen and Carbon Monoxide Directly by IR Spectroscopy. *J. Org. Chem.* **2006**, *71*, 6357-6367.

(32) Oomens, J.; Bakker, J. M.; Sartakov, B. G.; Meijer, G.; von Helden, G. The Infrared Spectrum of the Benzoyl Cation. *Chem. Phys. Lett.* **2003**, *367*, 576–580.

(33) Patzer, A.; Chakraborty, S.; Dopfer, O. Infrared Spectra and Quantum Chemical Characterization of Weakly Bound Clusters of the Benzoyl Cation with Ar and H_2O. *Phys. Chem. Chem. Phys.* **2010**, *12*, 15704–15714.

(34) Zhao, Y.; Truhlar, D. G. The M06 Suite of Density Functionals for Main Group Thermochemistry, Thermochemical Kinetics, Noncovalent Interactions, Excited States, and

Transition Elements: Two New Functionals and Systematic Testing of Four M06-class Functionals and 12 Other Functionals. *Theor. Chem. Acc.* **2008**, *120*, 215-241.

(35) Dunning, T. H. Gaussian Basis Sets for Use in Correlated Molecular Calculations. I. The Atoms Boron through Neon and Hydrogen *J. Chem. Phys*. **1989**, *90*, 1007-1023.

(36) Frisch, M. J.; Trucks, G. W.; Schlegel, H. B.; Scuseria, G. E.; Robb, M. A.; Cheeseman, J. R.; Scalmani, G.; Barone, V.; Mennucci, B.; Petersson, G. et al.; Gaussian 09, Revision D.01, Gaussian Inc., Wallingford, CT, **2009**.

(37) Finley, J.; Malmqvist, P.- Å.; Roos, B. O.; Serrano-Andrés, L. The Multi-State CASPT2 Method. *Chem. Phys. Lett*. **1998**, *288*, 299-306.

(38) Aquilante, F.; De Vico, L.; Ferre, N.; Ghigo, G.; Malmqvist, P.- Å.; Neogrády, P.; Pedersen, T. B.; Pitoňák, M.; Reiher, M.; Roos, B. O.; Serrano-Andrés, L.; Urban, M.; Veryazov, V.; Lindh, R. MOLCAS 7: The Next Generation. *J. Comput. Chem*. **2010**, *31*, 224-247.

(39) Western, C. M. Pgopher, version 7.1.108, University of Bristol, **2010**, http://pgopher.chm.bris.ac.uk.

(40) mass spectra from http://webbook.nist.gov/chemistry/

Chart 1. Structures and ground state energies (kJ/mol) of the most stable isomers of $C_7H_4O_2^+$ calculated at the M06-2X/cc-pVTZ level.

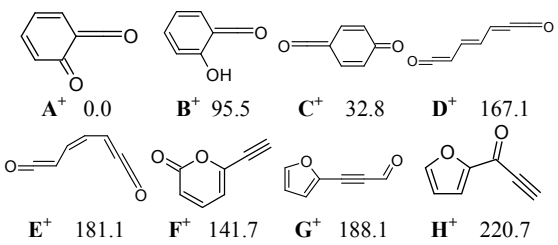

Chart 2. Structures and ground state energies (kJ/mol) of the $C_7H_5O_2^+$ isomers calculated at the M06-2X/cc-pVTZ level.

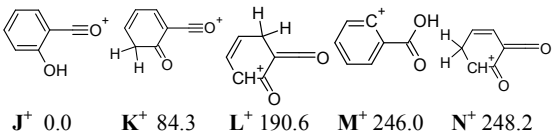

J$^+$ 0.0 **K**$^+$ 84.3 **L**$^+$ 190.6 **M**$^+$ 246.0 **N**$^+$ 248.2

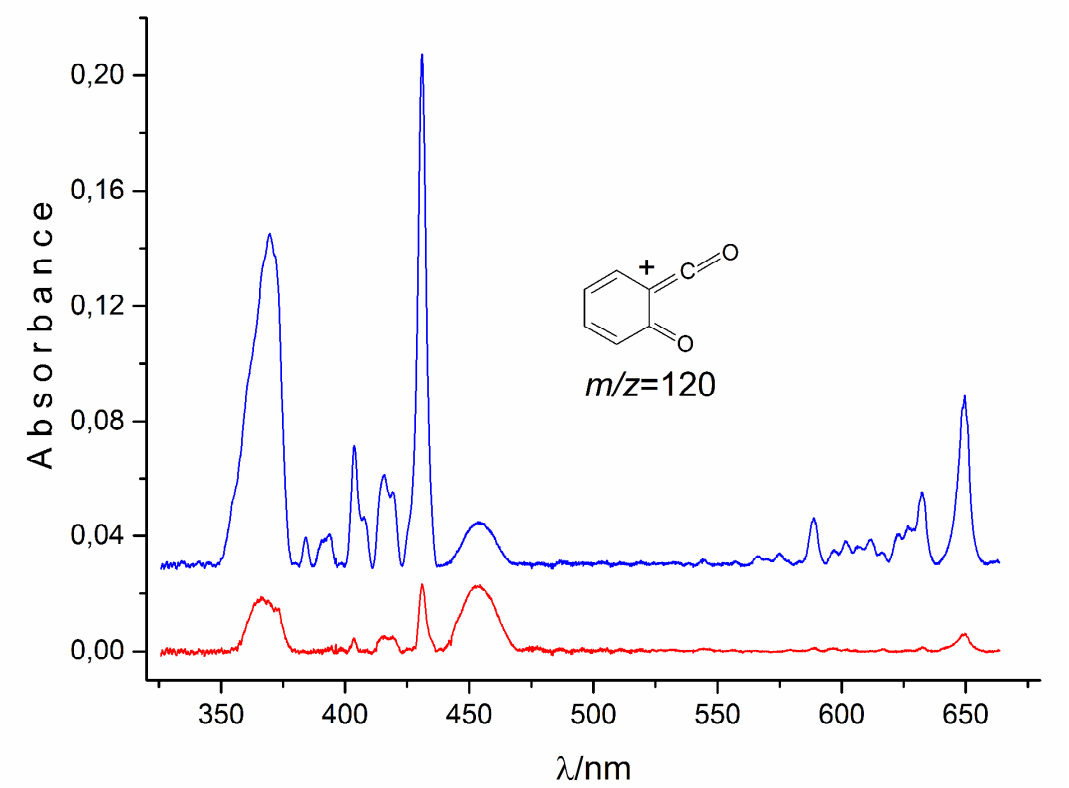

Figure 1. Absorption spectra measured after deposition of $C_7H_4O_2^+$ ions (*m/z* 120) in solid neon - blue trace, and after 30 min irradiation of the matrix with λ > 260 nm photons–red trace.

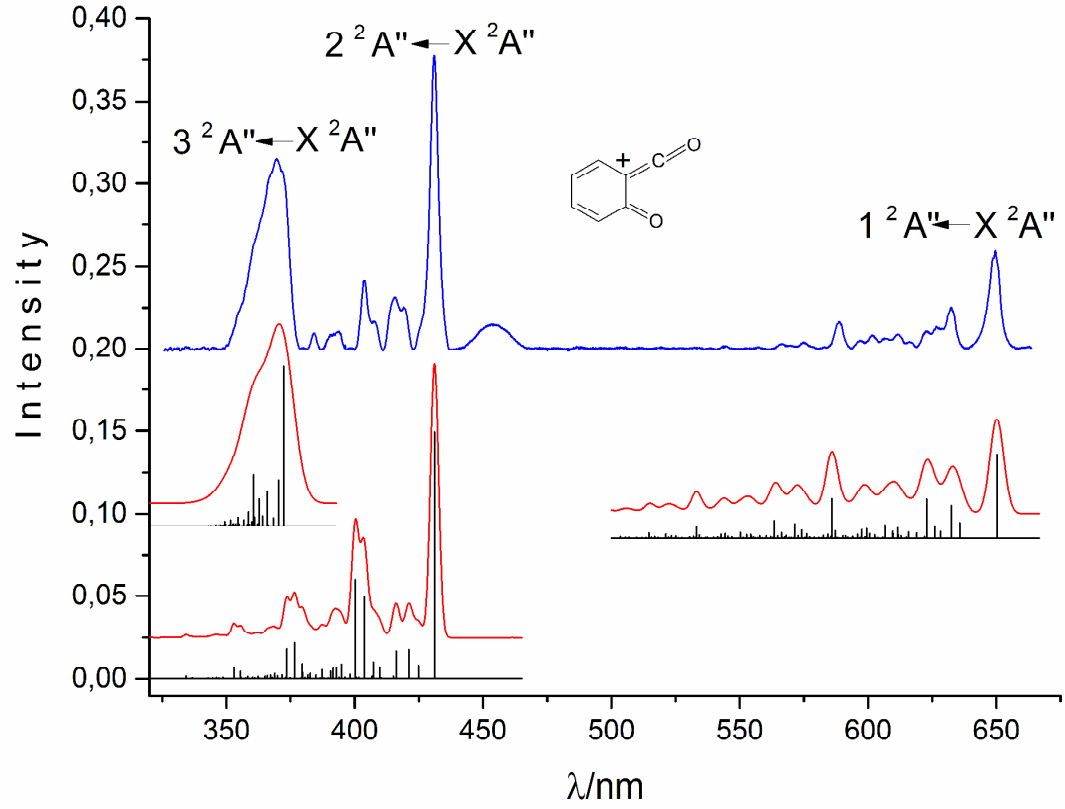

Figure 2. Electronic absorption spectrum of $C_7H_4O_2^+$ measured in a 6 K neon matrix compared with a Franck-Condon simulation for the transition from the ground X ^{2}A" to the 1 ^{2}A", 2 ^{2}A" and 3 ^{2}A" states. Red traces are obtained using 150, 200 and 750 cm^{-1} widths of individual vibronic bands.

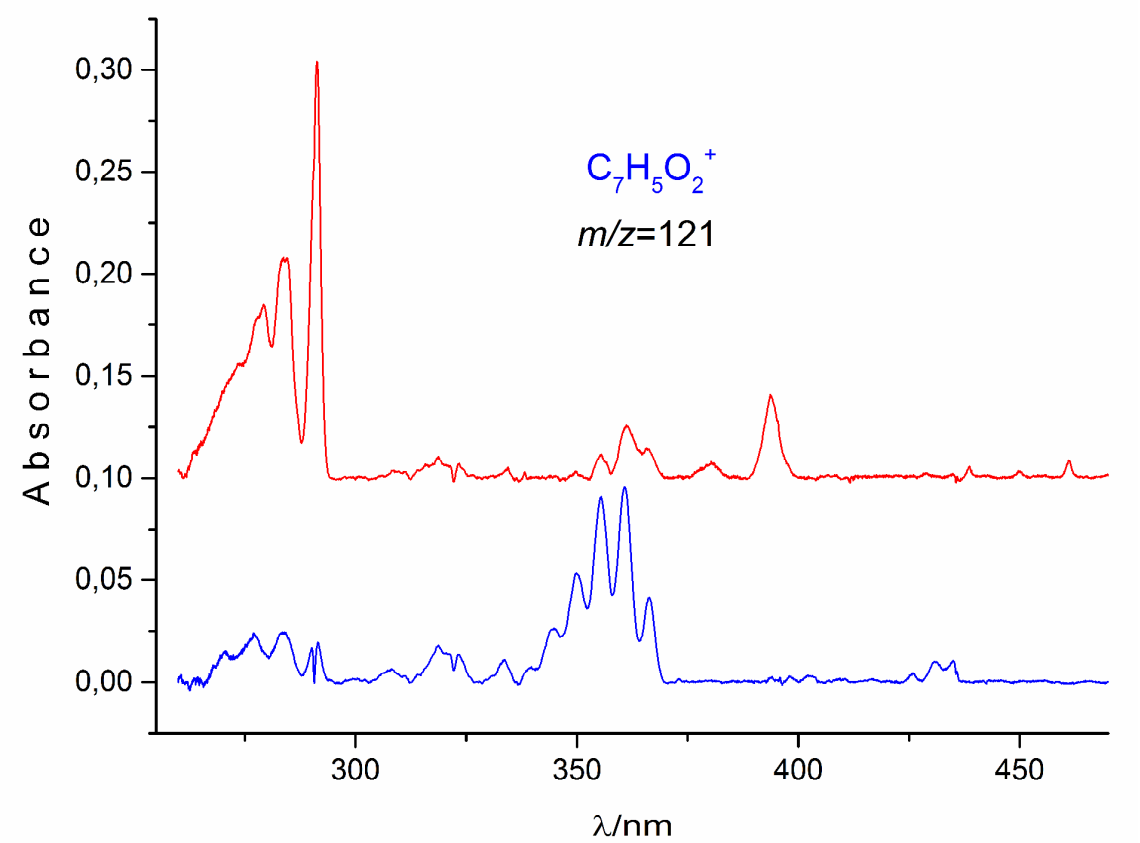

Figure 3. Electronic absorption spectrum of $C_7H_5O_2^+$ measured after deposition of *m/z* 121 ions in a 6 K neon matrix- blue trace, and the spectrum of neutral $C_7H_5O_2$ recorded after neutralization of the cations with $\lambda > 260$ nm photons - red trace.

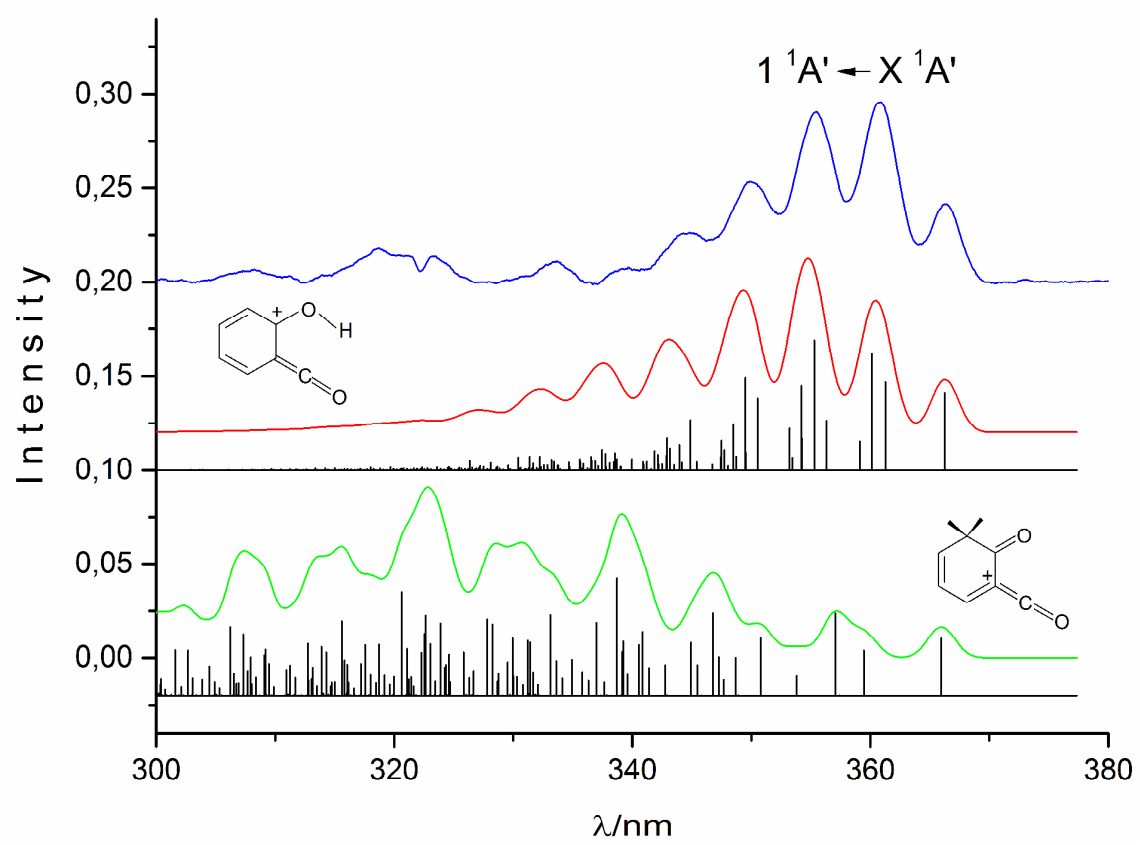

Figure 4. The neon matrix absorption spectrum of 2-hydroxybenzoyl cation – blue trace, compared with a Franck-Condon simulation of the transition for isomer $\mathbf{J}^+$ (middle panel): stick and Gaussian profiles of a 200 cm^{-1} width and for isomer isomer $\mathbf{K}^+$ - bottom panel.

Table 1. Comparison of the CASPT2 vertical excitation energies (eV) of the $C_7H_4O_2^+$ ($\mathbf{A}^+$) and $C_7H_5O_2^+$ ($\mathbf{J}^+$) ions and the respective neutrals with the energies derived from the spectra in a neon matrix.

Species	Transitions	Calc.	Exp.
$\mathbf{A}^+$	$1\,^2A'' \leftarrow X\,^2A''$	2.27	1.91
	$2\,^2A'' \leftarrow$	3.10	2.88
	$3\,^2A'' \leftarrow$	3.61	3.33
A	$1\,^1A' \leftarrow X\,^1A'$	3.55	2.74
$\mathbf{J}^+$	$1\,^1A' \leftarrow X\,^1A'$	3.87	3.38
J	$1\,^2A'' \leftarrow X\,^2A''$	2.48	2.69
	$2\,^2A'' \leftarrow$	3.38	3.15
	$3\,^2A'' \leftarrow$	3.83	3.43
	$4\,^2A'' \leftarrow$	4.99	4.26

Table 2. Observed band maxima (nm) of the cations and neutrals of $C_7H_4O_2$ and $C_7H_5O_2$ in 6 K neon matrices and assignment based on CASPT2 excitation energies and F-C simulations of vibrational profiles.

Species	λ/nm	$\tilde{\nu}$cm^{-1}	$\Delta\tilde{\nu}$/cm^{-1}	Assignment
$C_7H_4O_2^+$	649.6	15394	0	0_0^0 1 ^{2}A" ← X ^{2}A"
	632.5	15810	416	ν_{21}
	626.7	15957	563	ν_{19}
	622.6	16062	668	ν_{18}
	611.6	16351	957	ν_{16}
	606.4	16491	1097	$2\nu_{19}$
	601.4	16628	1234	$\nu_{19} + \nu_{18}$
	596.8	16756	1362	ν_{11}
	588.7	16987	1593	ν_7
	574.8	17397	2003	$\nu_7 + \nu_{21}$
	566.2	17662	2268	$\nu_7 + \nu_{18}$
	431.0	23202	0	0_0^0 2 ^{2}A" ← X ^{2}A"
	419.3	23849	647	ν_{19}
	415.4	24073	871	ν_{17}
	407.7	24528	1326	ν_{11}
	403.7	24771	1569	ν_8
	393.6	25407	2205	ν_5
	384.0	26042	2840	$\nu_5 + \nu_{19}$
	372.0	26882	0	0_0^0 3 ^{2}A" ← X ^{2}A"
$C_7H_4O_2$	453.0	22075	0	0_0^0 1 ^{1}A' ← X ^{1}A'
$C_7H_5O_2^+$	366.4	27293	0	0_0^0 1 ^{1}A' ← X ^{1}A'
	360.8	27716	423	ν_{24} and ν_{23}
	355.5	28129	836	ν_{19} , $\nu_{24} + \nu_{23}$
	350.0	28571	1278	ν_{15}
	344.9	28994	1701	ν_8, $\nu_{24} + \nu_{19}$
	339.0	29499	2206	ν_7
	333.4	29994	2701	
$C_7H_5O_2$	461.2	21683	0	0_0^0 1^{2}A" ← X ^{2}A"
	449.9	22227	544	ν_{22}
	438.5	22805	1122	$2\nu_{22}$
	393.8	25394	0	0_0^0 2 ^{2}A" ← X ^{2}A"
	380.4	26288	894	ν_{18}
	361.2	27685	0	0_0^0 3 ^{2}A" ← X ^{2}A"
	355.5	28129	444	ν_{23}
	291.3	34329	0	0_0^0 4 ^{2}A" ← X ^{2}A"
	290.4	34435	106	ν_{25}
	284.9	35096	767	ν_{20}
	283.1	35323	994	ν_{18}
	279.3	35804	1475	

Table of Contents graphic

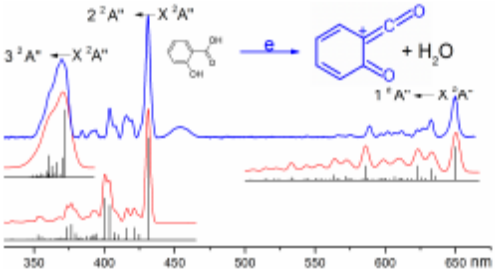

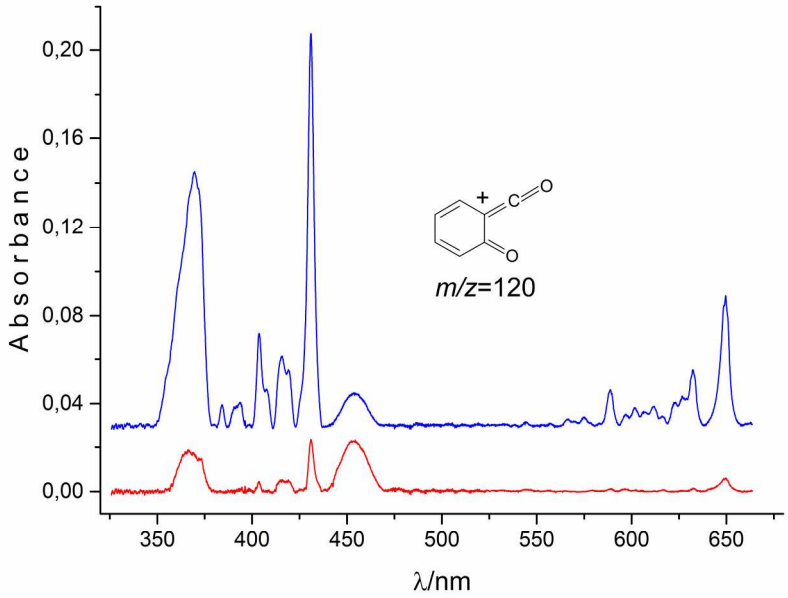

Figure1

209x148mm (300 x 300 DPI)

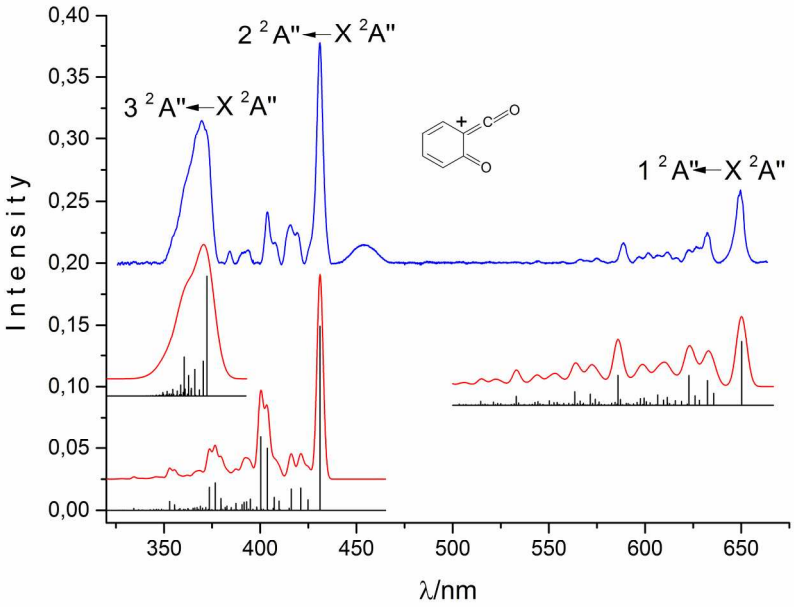

Figure2

209x148mm (300 x 300 DPI)

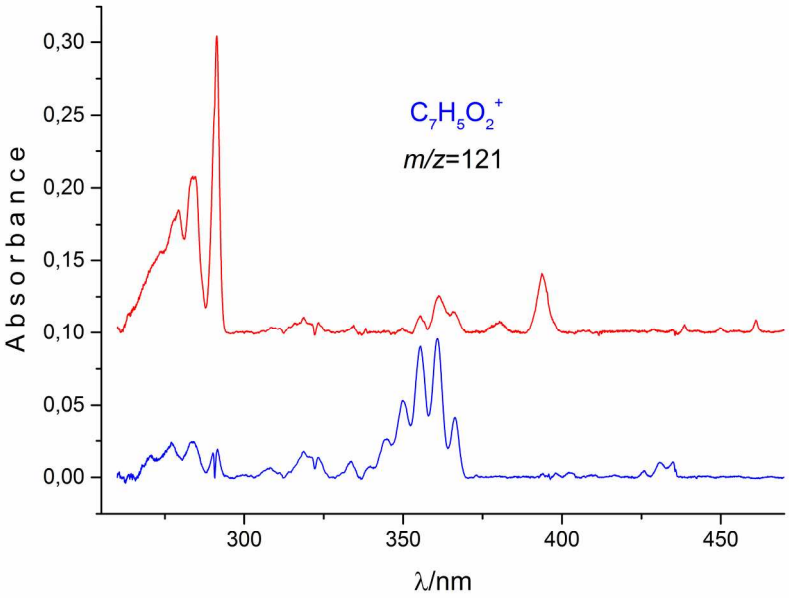

Figure3

209x148mm (300 x 300 DPI)

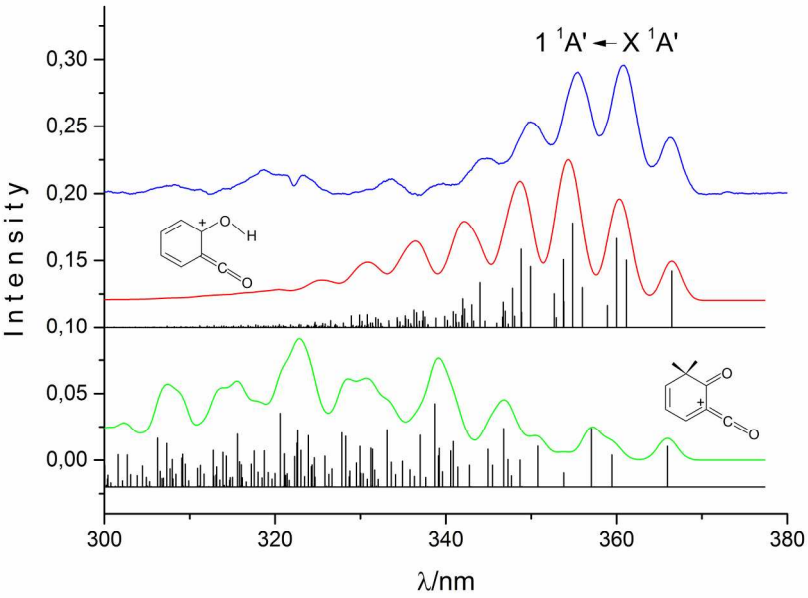

Figure4

209x148mm (300 x 300 DPI)

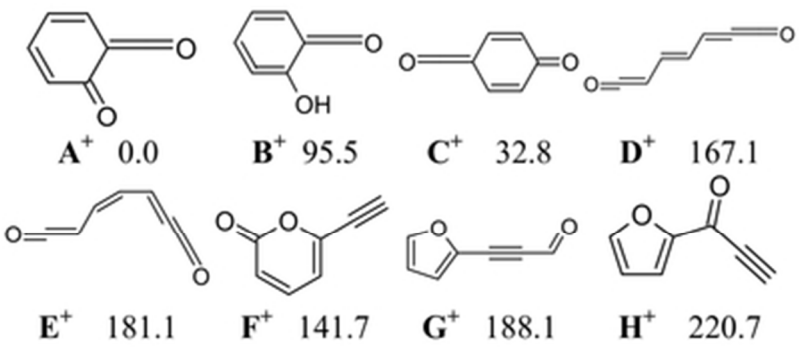

Chart1

33x14mm (300 x 300 DPI)

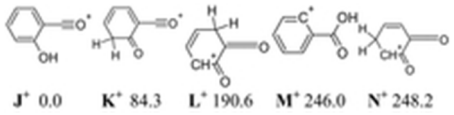

Chart2

18x4mm (300 x 300 DPI)

Species	Transitions	Calc.	Exp.
$\mathbf{A}^+$	$1\,^2A'' \leftarrow X\,^2A''$	2.27	1.91
	$2\,^2A'' \leftarrow$	3.10	2.88
	$3\,^2A'' \leftarrow$	3.61	3.33
A	$1\,^1A' \leftarrow X\,^1A'$	3.55	2.74
$\mathbf{J}^+$	$1\,^1A' \leftarrow X\,^1A'$	3.87	3.38
J	$1\,^2A'' \leftarrow X\,^2A''$	2.48	2.69
	$2\,^2A'' \leftarrow$	3.38	3.15
	$3\,^2A'' \leftarrow$	3.83	3.43
	$4\,^2A'' \leftarrow$	4.99	4.26

Table1

43x27mm (300 x 300 DPI)

Species	λ/nm	$\tilde{\nu}$cm^{-1}	$\Delta\tilde{\nu}$/cm^{-1}	Assignment
$C_7H_4O_2^+$	649.6	15394	0	0_0^0 1 ^{2}A" ← X ^{2}A"
	632.5	15810	416	ν_{21}
	626.7	15957	563	ν_{19}
	622.6	16062	668	ν_{18}
	611.6	16351	957	ν_{16}
	606.4	16491	1097	$2\nu_{19}$
	601.4	16628	1234	$\nu_{19} + \nu_{18}$
	596.8	16756	1362	ν_{11}
	588.7	16987	1593	ν_7
	574.8	17397	2003	$\nu_7 + \nu_{21}$
	566.2	17662	2268	$\nu_7 + \nu_{18}$
	431.0	23202	0	0_0^0 2 ^{2}A" ← X ^{2}A"
	419.3	23849	647	ν_{19}
	415.4	24073	871	ν_{17}
	407.7	24528	1326	ν_{11}
	403.7	24771	1569	ν_8
	393.6	25407	2205	ν_5
	384.0	26042	2840	$\nu_5 + \nu_{19}$
	372.0	26882	0	0_0^0 3 ^{2}A" ← X ^{2}A"
$C_7H_4O_2$	453.0	22075	0	0_0^0 1 ^{1}A' ← X ^{1}A'
$C_7H_5O_2^+$	366.4	27293	0	0_0^0 1 ^{1}A' ← X ^{1}A'
	360.8	27716	423	ν_{24} and ν_{23}
	355.5	28129	836	ν_{19} , $\nu_{24} + \nu_{23}$
	350.0	28571	1278	ν_{15}
	344.9	28994	1701	$\nu_{8,}$ $\nu_{24} + \nu_{19}$
	339.0	29499	2206	ν_7
	333.4	29994	2701	
$C_7H_5O_2$	461.2	21683	0	0_0^0 1^{2}A" ← X ^{2}A"
	449.9	22227	544	ν_{22}
	438.5	22805	1122	$2\nu_{22}$
	393.8	25394	0	0_0^0 2 ^{2}A" ← X ^{2}A"
	380.4	26288	894	ν_{18}
	361.2	27685	0	0_0^0 3 ^{2}A" ← X ^{2}A"
	355.5	28129	444	ν_{23}
	291.3	34329	0	0_0^0 4 ^{2}A" ← X ^{2}A"
	284.0	35211	882	ν_{18} or ν_{19}
	279.3	35804	1475	ν_9 or ν_{10}

Table2

148x279mm (300 x 300 DPI)